Prediction of H 2 S solubility in aqueous NaCl solutions by molecular simulation

Rémi Fauve, Xavier Guichet, Véronique Lachet, Nicolas Ferrando

Prediction of H_2S solubility in aqueous NaCl solutions by molecular simulation

Rémi Fauve[1], Xavier Guichet[1], Véronique Lachet[1,2], Nicolas Ferrando[1,*]

[1] IFP Energies nouvelles, 1 et 4 avenue de Bois-Préau, 92852 Rueil-Malmaison, France

[2] Laboratoire de Chimie Physique, Université Paris-Sud, UMR 8000 CNRS, Orsay, France

Abstract

The solubility of hydrogen sulfide in aqueous NaCl solutions has been investigated by calculation of Henry constants through Monte Carlo simulations and using a nonpolarizable force field. The Lorentz-Berthelot combining rules appeared the most appropriate to simulate this system compared to other usual rules. The physical behavior and the trends experimentally observed are qualitatively well reproduced by this purely predictive approach for the binary system H_2S+H_2O as well as for the salted system H_2S+H_2O+NaCl: as experimentally expected, the simulations indicate a maximum in the Henry constant curve with temperature and an increase of the Henry constant with the salt concentration (salting-out effect). From a quantitative point of view, Henry constants are systematically overestimated, and more specifically for high temperatures. By introducing an empirical temperature-independent binary interaction coefficient between water and hydrogen sulfide, it is possible to obtain a good agreement between experiments and calculated Henry constants for both salt-free and salted systems, over a large temperature range (290 to 590 K) and salinity ranging from 0 to 6 mol/kg. For temperatures less than 400 K, the deviations are smaller and within the experimental uncertainties. At higher temperatures, deviations are higher but only few experimental data are available to confirm this result. Considering statistical and experimental uncertainties, this approach can thus provide a reasonable estimation of H_2S solubility in NaCl aqueous solution in conditions encountered in geological formations. For a given temperature, the variation of the Henry constant with salt concentration is not exactly the same as the variation experimentally observed, and the salting-out effect is overestimated. This suggests for future works that additional forces such as polarization have to be taken into account for modeling high salt concentration systems.

Keywords: hydrogen sulfide; NaCl; solubility; Henry constant; Monte Carlo simulation

* Corresponding author : nicolas.ferrando@ifpen.fr

1. Introduction

Hydrogen sulfide (H_2S), produced in natural geological formation by the thermo-reduction of the sulfates (TSR), presents serious hazards when liberated in important quantities. The separation of H_2S from methane and other hydrocarbons is an important step in the treatment of a natural gas at the production site before transport, and represents important costs. The petroleum industry is therefore interested by the assessment of the reservoir H_2S content at the beginning of the exploration phase. To properly address the H_2S transport in geological formations, the dissolved amount of H_2S in formation waters has to be estimated. To calculate phase equilibrium of H_2S + brine systems, actually most of the available basin or reservoir modeling tools use empirical correlations (e.g. Barta and Bradley, 1985; Savary et al., 2012; Suleimenov and Krupp, 1994), activity coefficient models (e.g. Barrett et al., 1988; Dubessy et al., 2005; Li et al., 2014; Xia et al., 2000) or equations of state (e.g. Duan et al., 1996; Duan et al., 2007; Li et al., 2015; Soreide and Whitson, 1992; Ziabakhsh-Ganji and Kooi, 2012; Zirrahi et al., 2012). Such models require a large number of experimental data to be calibrated. A recent compilation (Koschel et al., 2013) indicates that around 700 experimental data of H_2S solubility in NaCl aqueous solutions are available in literature (Barrett et al., 1988; Douabul and Riley, 1979; Drummond, 1981; Kozintseva, 1963; Savary et al., 2012; Suleimenov and Krupp, 1994; Xia et al., 2000), but three quarters of them are for pressures less than 5 MPa. Actually the maximum experimental pressure investigated for H_2S solubility in brine is close to 30 MPa (Koschel et al., 2013; Savary et al., 2012), and the temperatures investigated are in a large majority less than 393 K, very far from conditions encountered in geological formations where TSR is expected to occur (Machel, 2001). Due to high toxicity and corrosiveness of this gas, experiments at high pressure are hazardous and expensive. Alternatives to experiments are thus recommended to evaluated H_2S solubility in severe temperature and pressure conditions.

For many years, molecular simulation has become a powerful tool to predict phase equilibrium of systems of industrial interest through Monte Carlo simulation techniques (Theodorou, 2010; Ungerer et al., 2005). The physical properties of aqueous electrolyte solutions have been widely studied in molecular simulation, and two kinds of force fields are commonly used: polarizable force fields and non-polarizable force fields. Using polarizable force fields to simulate water+salt systems (e.g. Jiang et al., 2015; Jiang et al., 2016; Kiss et al., 2012b; Kiss et al., 2012a; Kiss and Baranyai, 2014; Lamoureux and Roux, 2006; Moučka et al., 2013, 2015; Neyt et al., 2013; Rick et al., 1994; Yu et al., 2010) allows a better representation of interactions between centers of force and is expected to improve quantitative accuracy, but this approach is time consuming. Non-polarizable force fields have the benefit of greater simplicity and helps to save computation time for this system (e.g. Lísal et al., 2005; Mester and Panagiotopoulos, 2015; Moucka et al., 2013; Orozco et al., 2014). Although the water+salt system has been widely investigated in molecular simulation, the simulation of gas solubility in aqueous electrolyte solutions remains scarce and challenging due to high complexity of molecular interactions involving ionic species. Prior studies on this topic mainly concern CO_2 solubility in NaCl or $CaCl_2$ solutions (Liu et al., 2013; Tsai et al., 2016; Vorholz et al., 2004). To the best of our knowledge, no study dealing with the H_2S solubility in aqueous electrolyte solution by molecular simulation has been published in open literature. Hence, the goal of this work is to evaluate existing non-polarizable force fields and methodologies to predict H_2S solubility in aqueous NaCl solutions from 0 to 6 mol/kg by Monte Carlo simulations, and to identify the actual limitations of the evaluated approach. In the first part of this paper, a review of available experimental data on

both salt-free and salted systems is carried out and optimized parameters are proposed to correlate these data. The second part deals with the molecular models and the combining rules used for the simulations, and with the simulation techniques employed to compute the Henry constants of H_2S in pure and salted water. The results obtained either for the binary system H_2S+H_2O or the ternary system H_2S+H_2O+NaCl are discussed in the third part. Conclusions and perspectives are provided in the last section.

2. Review of available experimental data

2.1 The binary system H_2S+H_2O

For the binary system H_2S+H_2O, literature provides a large number of experimental data, mainly given either in terms of Henry constant H_i (Rinker and Sandall, 2000), or in terms of H_2S solubility x_i (molar fraction) (Barrett et al., 1988; Burgess and German, 1969; Chapoy et al., 2005; Gerrard, 1972; Koschel et al., 2007; Kuranov et al., 1996; Lee and Mather, 1977; Pohl, H. A., 1961; Selleck et al., 1952; Suleimenov and Krupp, 1994; Yu et al., 1980). At infinite dilution ($x_i \to 0$), the solubility and the Henry constant are linked by the following relationship:

$$H_i = \frac{f_i^{vap}}{x_i} = \frac{p_i \varphi_i^{vap}}{x_i} \qquad (1)$$

Where f_i^{vap} is the fugacity of the solute in the vapor phase, p_i is its partial pressure and φ_i^{vap} its fugacity coefficient in the vapor phase.

In this work, all the experimental data have been gathered in terms of H_2S Henry constant in water. Experimental data provided in terms of molar fraction have been converted in Henry constant using equation (1), and the Soave-Redlich-Kwong equation of state (Soave, 1972) to estimate the vapor fugacity coefficient of pure H_2S. To evaluate the experimental uncertainty, a correlation is used to smooth these experimental data. Harvey (Harvey, 1996) proposed a widely used correlation involving the critical temperature and the vapor pressure of water. We propose to use in this work the extension of the Harvey correlation proposed by Trinh et al. (Trinh et al., 2016) which allows a better extrapolation at high temperature:

$$T_r \ln \frac{H_i}{P^{\sigma}_{solvent}} = a_i + b_i \left(1 - T_r\right)^{0.355} + c_i T_r \left(\frac{1}{T_r} - 1\right)^{1.5} \qquad (2)$$

where $P^{\sigma}_{solvent}$ is the pure water vapor pressure, and T_r=T/T_c the water reduced temperature, with T_c=647.096 K the critical temperature of water. The empirical parameters a_i, b_i and c_i are adjusted on all experimental data (158 points ranging from 273.15 to 563.15 K), and are provided in Table 1.

Figure 1 shows the raw experimental data and the adjusted correlation. The average deviation between experimental and smoothed data is about ±25% and that can be considered as an order of magnitude of the experimental uncertainties. A maximum of the Henry constant is observed for T = 450 K. The number of experimental measurements decreases with increasing temperature, so that

experimental values are scarce for temperatures higher than 500 K. This correlation and its uncertainty will be used for further comparisons with simulation results.

2.2 The ternary system H_2S+H_2O+NaCl

Experimental data of Henry constant or solubility of H_2S in aqueous NaCl solutions are mainly provided at atmospheric pressure and low temperature (Barrett et al., 1988), far from conditions encountered in natural geological formations. Some data are available at higher temperatures, such as solubility measured by Koschel *et al.* (Koschel et al., 2013) (up to 353.15 K and 5 mol/kg for salinity), Xia *et al.* (Xia et al., 2000) (up to 393.15 K and 6 mol/kg for salinity) and Henry constants reported by Suleimenov *et al.* (Suleimenov and Krupp, 1994) (from 428 to 593 K and salinity up to 2 mol/kg). Experiments show that the solubility of H_2S tends to decrease when salt is added in the system: this is the well-known salting-out effect. This effect is often correlated using an empirical function $f\left(T, m_{sel}\right)$ linking the solubility of the gas in the salt-free system x_i and the solubility of the gas in the salted system x_i^*:

$$\ln \frac{x_i}{x_i^*} = f\left(T, m_{salt}\right) \qquad (3)$$

Where m_{salt} stands for the salt molality (mol/kg of solvent).

One of the most widely function used is the Setschenow form (Setschenow, 1889), providing a linear dependency of the logarithm of the solubility ratio with the salt concentration:

$$\ln \frac{x_i}{x_i^*} = k_s m_{salt} \qquad (4)$$

where k_s is the Setschenow coefficient.

However, some preliminary attempts to correlate the available experimental data with this simple equation showed that a more complex function should be used to obtain a satisfactory accuracy. Since the solubility ratio is related to the change in activity observed when salt is added in the system, we propose in this work to use a correlation inspired from the Drummond's activity coefficient model developed for neutral species in brines (Drummond, 1981):

$$\ln \frac{x_i}{x_i^*} = \left(C + F \cdot T + \frac{G}{T}\right) m_{salt} - \left(E + H \cdot T\right)\left(\frac{m_{salt}}{m_{salt}+1}\right) \qquad (5)$$

Where *C*, *F*, *G*, E and *H* are empirical parameters equal to -1.0312, 0.0012806, 255.9, 0.4445 and -0.001606, respectively, in the original work. In order to obtain the best possible agreement, parameters C and E are refitted considering all the experimental data available for temperatures ranging from 298 to 428 K, pressures less than vapor pressure of the solvent and salinity values up to 6 mol/kg. In these conditions of moderate pressures, the gas phase behaves like an ideal gas, and the fugacity coefficient in equation (1) can be taken equal to 1. For an experimental value of $x_{H_2S}^*$, the

corresponding value of x_{H_2S} in pure water at the same temperature and partial pressure is calculated from equation (1) and (2). The optimal values found for parameters C and E are equal to -1.113 and 0.3576, respectively. Figure 2 shows parity diagram between experimental data and calculated data with equation (5).

Finally, for a given H_2S partial pressure and at infinite dilution, Henry constants and solubilities in salt-free and salted systems are related by:

$$\frac{H_i^*}{H_i} = \frac{x_i}{x_i^*} \qquad (6)$$

Since the experimental data are scarce for temperatures greater than 400 K and for particularly high salinity brine (greater than 1 mol/kg), the Henry constant in salted systems will be assessed by using equations (5) and (6) and will be used as reference data to evaluate results obtained from molecular simulation.

3. Simulation methods

3.1 Force field

The molecular model used for hydrogen sulfide is the model of Kristof and Liszi (Kristof and Liszi, 1997) which involves one Lennard-Jones center and four electrostatic charges. This model allows to obtain a good accuracy for prediction of vapor pressures, saturated liquid densities and vaporization enthalpies of pure H_2S (Kristof and Liszi, 1997; Ungerer et al., 2004). For water, the SPC/E model (Berendsen et al., 1987) is used since prior studies showed good results in the prediction of aqueous electrolyte properties with this model (Ji et al., 2012; Tsai et al., 2016). For Na^+ and Cl^- ions, the OPLS model is used (Chandrasekhar et al., 1984). This choice is motivated by the fact that when coupled with the SPC/E model of water, this combination gives a reasonable prediction of the solution density on a large range of temperature (from 298 to 548 K). The densities calculated for NaCl molality of 1, 3 and 5 mol/kg in the NPT ensemble are plotted on Figure 3, and the average deviations between calculated and experimental density data (Apelblat and Manzurola, 1999; Romankiw and Chou, 1983; Zhang and Han, 1996) is equal to 1%.

Finally, the Table 2 provides details of the molecular models used.

As molecules are assumed to be rigid, only intermolecular interactions are accounted for in the potential energy calculation. Dispersion-repulsion interactions between force centers *i* and *j* are modeled with a 6-12-Lennard-Jones potential with a spherical cut-off equal to the half of the simulation box, and the classical tail correction is employed (Allen and Tildesley, 1987) :

$$U_{ij}^{LJ} = 4\varepsilon_{ij}\left[\left(\frac{\sigma_{ij}}{r_{ij}}\right)^{12} - \left(\frac{\sigma_{ij}}{r_{ij}}\right)^{6}\right] \qquad (7)$$

Where r_{ij} is the distance between the two force centers and ε_{ij} and σ_{ij} the energy and diameter parameters of the Lennard-Jones potential, respectively.

The electrostatic energy between two charges *i* and *j* is modeled with a Coulomb potential:

$$U_{ij}^{el} = \frac{q_i q_i}{4\pi\varepsilon_0 r_{ij}} \qquad (8)$$

Where ε_0 is the vacuum permittivity. For long-range corrections, the Ewald summation technique is used, with a number of reciprocal vectors k ranging from -7 to 7 in all three directions and a Gaussian width α equal to 2 in reduced units. Finally, no explicit polarization interactions are considered in this force field.

For the calculation of the cross Lennard-Jones parameters ε_{ij} and σ_{ij}, the Lorentz-Berthelot combining rules have been used for interactions between ions + water and ions + H_2S. For the interactions between water and H_2S, three usual combining rules (Lorentz-Berthelot, Kong (Kong, 1973) and Waldmann-Hagler (Waldmann and Hagler, 1993)), described in Table 3, are evaluated in this work on the phase equilibrium calculation of the binary system H_2S + H_2O. This choice is motivated by the fact that the Lorentz-Berthelot combining rules are widely used in molecular simulation, and the Kong and Waldmann-Hagler combining rules yielded good accuracy in phase equilibrium of systems involving light gases (Delhommelle and Millie, 2001; Ungerer et al., 2004; Waldmann and Hagler, 1993).

As discussed later, an empirical correction of the Lorentz-Berthelot combining rule is also possible by introducing a binary interaction parameter k_{ij}, generally adjusted to minimize the deviations between experimental and calculated selected properties:

$$\varepsilon_{ij} = \sqrt{\varepsilon_i \varepsilon_j} \cdot \left(1 - k_{ij}\right) \qquad (9)$$

3.2 Algorithms

By definition, the fugacity of a solute in a liquid phase f_i^{liq} is related to its chemical potential μ_i^{liq} by the relation:

$$f_i^{liq} = f_i^0 \exp\left(\frac{\mu_i^{liq} - \mu_i^0}{RT}\right) \qquad (10)$$

Where the superscript *0* stands for the reference state, *R* is the ideal gas constant and *T* is the temperature.

The choice of the reference state is fully arbitrary. In this work, the reference state (zero chemical potential) corresponds to an hypothetical pure ideal gas of unit density (1 molecule per Å^3, i.e. a density ρ^0=1.66·10^6 mol/m^3). The fugacity in this reference state f_i^0 is then equal to $\rho^0 RT$.

As the phase equilibrium condition imposes:

206 $$f_i^{vap} = f_i^{liq} \quad (11)$$

207 the Henry constant defined by equation (1) can be determined by:

208 $$H_i = \frac{f_i^0}{x_i} \exp\left(\frac{\mu_i^{liq} - \mu_i^0}{RT} \right) \quad (12)$$

209 Thus, the Henry constant can be calculated by molecular simulation with any simulation algorithm
210 allowing the evaluation of the excess chemical potential $\mu_i^{ex} = \mu_i^{liq} - \mu_i^0$ of the solute in the liquid
211 phase.

212

213 **3.2.1 Widom particle insertion algorithm**
214

215 In this work, the first algorithm used to evaluate the chemical potential is the so-called Widom
216 particle insertion method (Frenkel and Smit, 1996; Widom, 1963), a smart algorithm allowing the
217 computation of the excess chemical potential through molecular simulations. In this method, the
218 excess chemical potential is calculated by the following ensemble average:

219 $$\mu_i^{ex} = -k_B T \ln \left\langle \frac{PV}{k_B T (N+1)} \exp\left(-\frac{\Delta U}{k_B T} \right) \right\rangle_{NPT} \quad (13)$$

220 Where k_B is the Boltzmann constant, ΔU is the potential energy difference due to the insertion of
221 the test molecule *i*, and *T*, *P*, *V*, and *N* are respectively the temperature, pressure, volume and
222 number of molecule in the system.

223 The Monte Carlo simulations are carried out in the NPT statistical ensemble. For each temperature
224 studied, the pressure of the system is taken equal to the vapor pressure of the solvent. For salt-free
225 systems, a total number of 520 water molecules is used. For salted system, the total number of water
226 molecules and ions is taken around 700, the number of Na^+ and Cl^- ions being adjusted to obtain the
227 desired salt concentration in the liquid phase. The chemical potential is computed during a
228 production run lasting for typically 50 million and 100 million Monte Carlo steps in salt-free and
229 salted systems, respectively. One step corresponds to a single Monte Carlo move. Before each
230 production run, a preliminary run lasting for 50 (salt-free systems) to 100 (salted systems) million
231 Monte Carlo steps is carried out to achieve equilibrium. The different Monte Carlo moves and their
232 corresponding attempt probabilities used during simulations are molecular translation (20%),
233 molecular rotation (20%), volume change (0.5%) and insertion test (59.5%), with a preinsertion
234 statistical bias (Mackie et al., 1997). The amplitude of translations, rotations and volume changes are
235 adjusted during the simulation to achieve an acceptance ratio of 40%. The simulations were carried
236 out using the GIBBS software jointly developed by IFP Energies nouvelles and the Laboratoire de
237 Chimie Physique (CNRS-Université Paris-Sud) (Ungerer et al., 2005).

238

3.2.2 Thermodynamic integration algorithm

The simulations of the salted systems at high salt concentration yield to a dense and well-structured liquid phase. From a simulation point of view, the insertion of a molecule of H_2S in the liquid phase becomes more difficult and the convergence of a simulation longer to reach. In order to validate the results obtained with the previous Widom insertion particle algorithm in the aqueous NaCl solutions, the Henry constant of H_2S is also evaluated with an alternative method: the thermodynamic integration algorithm (Frenkel and Smit, 1996). This method allows the computation of the Gibbs energy of solvation of a solute ΔG_i^{solv} which is linked to the Henry constant of this solute by the following relationship (Ben-Naim, 1978):

$$H_i = RT\rho_s^{liq}\exp\left(\frac{\Delta G_i^{solv}}{RT}\right) \qquad (14)$$

Where ρ_s^{liq} is the molar liquid density of the solvent. This method is based on a gradual insertion of the solute in the solvent, avoiding thus the difficulties to insert directly a molecule in a dense phase. However, as described below, this gradual insertion requires a large number of Monte Carlo simulations for a single Henry constant computation. It is consequently an efficient but time-consuming method. The thermodynamic integration algorithm has been extensively described elsewhere (Economou et al., 2010; Garrido et al., 2009; Shirts et al., 2003), and only basics and simulation details are given here. As the Gibbs energy is a state function, it can be calculated from a thermodynamic cycle of non-physical transformations. Figure 4 describes the thermodynamic cycle used to calculate the Gibbs energy of solvation, defined as the energy difference of the solute in vacuum and in the solvent.

Following this cycle, the Gibbs energy of solvation is given by:

$$\Delta G^{solv} = \Delta G_{VdW}^{solvent} + \Delta G_{elec}^{solvent} + \Delta G^{dummy} - \Delta G^{vacuum} \qquad (15)$$

The terms $\Delta G_{VdW}^{solvent}$ and $\Delta G_{elec}^{solvent}$ correspond to the Gibbs energy of "insertion" of the bonded assembly of uncharged Lennard-Jones spheres and to the Gibbs energy required for "charging" the solute (Shirts et al., 2003). The term ΔG^{vacuum} corresponds to the same transformation, but in vacuum instead of solvent. It thus involves only intramolecular interactions. As the molecules considered in this work are rigid, this contribution is zero, as well as the contribution ΔG^{dummy} (Gibbs energy of a non-interacting rigid molecule). The thermodynamic integration method consists in evaluating a Gibbs energy difference using the following expression:

$$\Delta G = \int_0^1 \left\langle \frac{\partial U(\lambda)}{\partial \lambda} \right\rangle d\lambda \qquad (16)$$

where U is the interaction potential between solute and solvent, and λ a coupling variable: $\lambda = 1$ means a full coupling between the solute and the solvent molecules, while $\lambda = 0$ means that solute

does not interact with the solvent. As suggest by Beutler *et al.* (Beutler et al., 1994), a soft-core potential for dispersion-repulsion interactions between solute and solvent molecules is used:

$$U_{ij}^{disp-rep} = 4\varepsilon_{ij}\lambda_{VdW}^{n}\left[\frac{1}{\left[\alpha\left(1-\lambda_{VdW}\right)^{2}+\left(\frac{r_{ij}}{\sigma_{ij}}\right)^{6}\right]^{2}}-\frac{1}{\alpha\left(1-\lambda_{VdW}\right)^{2}+\left(\frac{r_{ij}}{\sigma_{ij}}\right)^{6}}\right] \quad (17)$$

Values of 0.5 and 4 are used for α and n, respectively (Shirts et al., 2003).

For the electrostatic energy the following coupling function is used (Chang, 2009; Garrido et al., 2010; Partay et al., 2005; Shirts et al., 2003):

$$U_{ij}^{elec} = \frac{\lambda_{C} q_i q_j}{4\pi\varepsilon_0 r_{ij}} \quad (18)$$

As a charge overlap could generate a singularity, the calculation of electrostatic energy for the various values of λ_C should be carried out for λ_{VdW} = 1 to ensure sufficient repulsion between atoms bearing electrostatic charges. The complete methodology can be summarized as follows. First, $\Delta G_{VdW}^{solvent}$ is calculated by fixing λ_C = 0 and by performing one Monte Carlo simulation per value of λ_{VdW}. The following 16 values of λ_{VdW} are selected: {0, 0.1, 0.2, 0.3, 0.35, 0.4, 0.425, 0.45, 0.475, 0.5, 0.55, 0.6, 0.7, 0.8, 0.9, 1}. Second, ΔG_{elec}^{solv} is calculated by fixing λ_{VdW} = 1 and by performing one Monte Carlo simulation per value of λ_C. The following 11 values of λ_C are selected: {0, 0.1, 0.2, 0.3, 0.4, 0.5, 0.6, 0.7, 0.8, 0.9, 1}. A Monte Carlo simulation consists in simulating a NPT ensemble at the desired temperature and the vapor pressure of the solvent, with one molecule of solute, and a total of around 700 molecules of water and ions. A simulation run lasted for 200 million steps, including an equilibrium run of 100 million steps. The different Monte Carlo moves and their corresponding attempt probabilities used during the simulations are molecular translation (50%), molecular rotation (49.5%), and volume change (0.5%).

4. Results and discussion

4.1 The binary system H_2S + H_2O

The simulation results obtained from Widom test insertion method with the three different combining rules (Lorentz-Berthelot, Kong and Waldmann-Hagler) are plotted on Figure 5. This figure clearly exhibits that the combining rules of Kong and Waldmann-Hagler strongly overestimate the

Henry constant of H_2S in pure water, and are not suitable to model this system accurately. Using the Lorentz-Berthelot rules also tends to overestimate experimental Henry constant but with a reduced deviation (average relative deviation of around 50%). This deviation remains higher than the estimated experimental uncertainties but it is worth noticing that with this purely predictive approach the variation of the Henry constant with temperature is qualitatively well reproduced, and more specifically the existence of a maximum at around 450 K.

For engineering needs, more quantitative results could be required. The use of an empirical binary interaction parameter k_{ij} in the Lorentz-Berthelot combining rule (equation (9)) is a possible way to reduce deviations with experiments, although strongly altering the predictive feature of the molecular simulation approach. A temperature-independent k_{ij} is adjusted on experimental Henry constant data, leading to an optimal value of -0.16. The simulations with this empirical parameter lead to average deviation of around 40%, still higher than experimental uncertainties. As illustrated on Figure 6, the calculated Henry constant with this optimal k_{ij} are underevaluated at low temperature and overestimated at high temperature. Thus, the appropriate empirical correction would be to introduce a temperature-dependent k_{ij}, and the following linear dependency has been optimized on experimental data:

$$k_{ij}(T) = -4.43 \cdot 10^{-4} \cdot T(K) + 0.103 \qquad (19)$$

In this case, the average deviation decreases to 19%, but the simulations are in no way predictive, and this approach will be no more considered further. To obtain a better accuracy with a fully predictive way, the force field has to be drastically modified. As Henry constant is overestimated (and consequently solubility underestimated), it could also be argued that neglecting the dissociation of H_2S into HS^- and S^{2-} in our modeling approach is not a correct assumption. However, considering an average dissociation constant of $9.6 \cdot 10^{-8}$ for the first acidity (Sun et al., 2008) , the concentration of HS^- remains less than 1% of the concentration of dissolved molecular H_2S for pH up to 5.5, and this cannot reasonably explain the overestimation observed.

4.2. The ternary system $H_2S + H_2O + NaCl$

The addition of salt makes the aqueous phase more dense and more structured due to the solvation of ions by the water molecules. This behavior can be visualized on the radial distribution functions (rdf) between H_2O-Na^+ pairs and H_2O-Cl^- pairs plotted on Figure 7. These rdf exhibit two large peaks at 2.4 and 3.3 Å, respectively, indicating a high probability to find water molecules at this short distance of ions. The integration of the denormalized rdf (coordination numbers) gives a total number of 6 water molecules surrounding a Na^+ ion and of 7 water molecules surrounding a Cl^- ion in the first solvation shell, determined by the location of the first minima in the rdf. This result is consistent with previous simulation studies (Impey et al., 1983; Lee and Rasaiah, 1996). Increasing temperature tends to decrease the coordination number due to thermal agitation. A decrease of about 10% in the coordination number of both Na^+ and Cl^- is observed by changing the temperature from 298 K to 548 K.

Figure 8 compares the Henry constants at 323.15 K and salinities from 0 to 5 mol/kg calculated using either the Widom test insertion method or the thermodynamic integration algorithm. Results obtained using the same force field are found very close and lie within the statistical uncertainties of these two methods (typically between +/-5 and +/-10 % for Widom test insertion and +/- 10 and +/- 20% for thermodynamic integration). For further calculations, the Widom particle insertion method will be systematically used since it allows a direct calculation of Henry constant in a single Monte Carlo simulation.

Figure 9 shows the variation of Henry constant of H_2S in a NaCl aqueous solution for three molal concentrations as a function of temperature. The Monte Carlo simulation results obtained with the predicted approach without k_{ij} are in green, while the ones obtained with the approach using the optimized H_2S-H_2O k_{ij} are in blue. For each molality, the available experimental data are plotted (red dots). The dash line is the correlated Henry constant of H_2S in pure water (eq. 2). The bold line is the correlated Henry constant of H_2S in aqueous solutions calculated according the approach described in section 2.2. The shaded grey area shows the minimal uncertainty associated to the experimental measurements.

The Monte Carlo simulation results obtained with the predicted approach clearly overestimate the Henry constants. The overestimation increases with increasing temperature (typically above 400 K), and with increasing salinity of the aqueous solution. It can be noticed that at high temperatures, only few experimental data are available. New experimental data could be useful to confirm or not this behavior. As shown in figure 1, our model underestimates densities at high temperature. But as an underestimation of density should theoretically lead to an underestimation of Henry constant, this cannot explain the overestimation observed. When using the previous optimal k_{ij} for the binary system H_2S+H_2O (k_{ij}=-0.16), results for the ternary system are found with a better quantitative agreement but remain overestimated at high temperatures (above 450 K)., As for the salt-free systems, experimental data exhibit a maximum, but shifted toward higher temperatures (above 500 K). The simulations are able to reproduce this behavior, with a maximum predicted close to 500 K.

Figure 10 shows the evolution of the H_2S Henry constant as a function of NaCl concentration for three isotherms (323.15, 353.15 and 393.15 K). Experimental data exhibit an increase of the Henry constant (and consequently a decrease of H_2S solubility) when salt concentration increases. This is the well-known “salting-out” effect, and simulation results qualitatively reproduce this behavior. Nevertheless the predictive approach without k_{ij} overestimates this effect, and more specifically at high salt concentration (above 3 mol/kg). The Henry constants obtained by Monte Carlo simulations with the approach using the optimized H_2S-H_2O k_{ij} are in fairly good agreement with the experimental data and this regardless the molality of the aqueous solution.

From a quantitative point of view, Table 4 provides for each temperature the average deviations obtained with both approaches evaluated. Without the binary interaction parameter, deviations are quite large, and this predictive approach has to be used only to estimate trends. When using the optimized H_2S-H_2O interaction coefficient, average deviations are reduced and of the same order of magnitude as the experimental uncertainties. Thus, considering the experimental and statistical uncertainties, this last approach allows to obtain a reasonable estimation of H_2S solubility in brines.

It makes clear that at high salt concentration, this nonpolarizable model fails to correctly describe the complex interactions in the electrolyte solution. The negative value for the k_{ij} indicates that the

attraction forces between H_2S and H_2O are presently underestimated. This suggests that attraction forces are missing in the force field, and a future improvement could consist in taking into account explicitly polarization forces. Furthermore, the effect of polarization forces will be more pronounced in high salt concentration solutions. The polarization energies due to cation P_+ and anion P_- in a solvent can be evaluated with (Misztal and Sangwal, 1999):

$$P = P_+ + P_- = -\frac{1}{2}e^2\left(1-\frac{1}{\varepsilon}\right)\left(\frac{1}{R_+}+\frac{1}{R_-}\right) \qquad (20)$$

With e is the elementary charge (e = 1.062·10^{-19} C), R_+ and R_- are the solvated ion radii in the solvent of dielectric constant ε. For Na^+, the solvated ionic radius is taken equal to 0.2356 ± 0.006 nm, and for Cl^-, the solvated radius is taken equal to 0.3187 ± 0.0025 nm (Marcus, 1988). The static dielectric constant for aqueous NaCl solutions is expected to decrease with increasing ionic concentrations (for instance at 25°C, the dielectric constant decreases from 78 to 35 for ionic concentrations increasing from 0 to 6 mol/kg) (Wang and Anderko, 2001). The evaluation of the polarization energy due to cations and anions in a NaCl aqueous solution, according to equation (20) for two temperatures (273 K and 323 K), as a function of the ionic concentration is shown in Figure 11. The magnitude of polarization energy is increasing linearly with the NaCl concentration, and is little affected by the temperature.

Figure 12 shows the radial distribution functions for Na^+-Cl^- ionic pairs in NaCl aqueous solutions for molalities ranging from 1 to 5 mol/kg. It clearly appears that the radial distribution exhibits a maximum around 2.9 Å for molalities greater than 3 mol/kg indicating the formation of ionic pairs in the solution. This behavior is consistent with observations made in prior studies on ion pairing in NaCl aqueous solutions (see e.g. (Chen and Pappu, 2007; Lyubartsev and Laaksonen, 1996)). It can be also generalized to other chloride salts, such as LiCl (e.g. (Chialvo and Simonson, 2007; Degreve and Mazzé, 2003), KCl (Chen and Pappu, 2007) or $CaCl_2$ (Megyes et al., 2006). The formation of these ionic pairs seems strongly affect the assessment of the Henry constant with the predictive approach, but has a lesser effect for the approach using the optimized H_2S-H_2O k_{ij}. This last observation may be linked to the behavior of the static dielectric constant with the salinity of NaCl solutions. For instance at 298 K, the static dielectric constant decreases strongly from 78 to ca. 45 for salinity ranging from 0 to 3 mol/kg, it decreases only from 45 to ca. 35 for salinity ranging from 3 to 6 mol/kg. The overall decrease of the static dielectric constant is linked to the formation of solvation layers (by water molecules). For aqueous solutions, the formation of hydration shells around ions prevents the "bound" water molecule from being oriented in the external electric field, thus causing a decrease of the dielectric constant. A further increase in the salt concentration (from 3 to 6 mol/kg) leads to a water deficit and to a redistribution of water molecules in the hydration shells, this levels off the decrease of the dielectric constant (Wang and Anderko, 2001).

All these observations seem to indicate that the use of a constant k_{ij} is well adapted to take into account the first order of the polarization corrections.

5. Conclusions

In this work, the solubility of hydrogen sulfide in aqueous NaCl solutions has been investigated by calculation of Henry constant through Monte Carlo simulations and Widom particle insertion method. A nonpolarizable force field is used, involving the SPC/E molecular model for water, the Kriztof and Liszi model for H_2S and the OPLS model for Na^+ and Cl^-. For the binary system H_2S+H_2O, the Lorentz-Berthelot combining rules appeared the most appropriate to simulate this system compared to other usual rules (Kong and Waldmann-Hagler). The physical behavior and the trends experimentally observed are qualitatively well reproduced by this purely predictive approach for the binary system H_2S+H_2O as well as for the salted system H_2S+H_2O+NaCl. Experimental data indicate a maximum in the Henry constant curve with temperature, close to 450 K for salt-free system and 500 K in an aqueous NaCl solution at 1 mol/kg, and the location of this maximum is well predicted by the simulations. Moreover, the "salting-out" effect experimentally observed is also predicted by our calculations. However, from a quantitative point of view, Henry constants are systematically overestimated, and more specifically for high temperatures. By introducing an empirical temperature-independent binary interaction coefficient between water and hydrogen sulfide, it is possible to obtain a quite good agreement between experiments and calculated Henry constants for both salt-free and salted systems, over a large temperature range (290 to 590 K) and salinity ranging from 0 to 6 mol/kg. For temperatures less than 400 K, the deviations are smaller and within the experimental uncertainties. At higher temperatures, deviations are higher but only few experimental data are available to confirm this result. Considering statistical and experimental uncertainties, this approach can thus provide a reasonable estimation of H_2S solubility in NaCl aqueous solution in conditions encountered in geological formations. For a given temperature, the variation of the Henry constant with salt concentration is not exactly the same as the variation experimentally observed, and the salting-out effect remains overestimated. This suggests for future works that additional forces such as polarization have to be taken into account for modeling high salt concentration systems.

References

Allen, M.P., Tildesley, D.J., 1987. Computer Simulation of Liquids. Oxford University Press.

Apelblat, A., Manzurola, E., 1999. Volumetric properties of water, and solutions of sodium chloride and potassium chloride at temperatures fromT=277.15 K toT=343.15 K at molalities of (0.1, 0.5, and 1.0)mol. J.Chem.Thermodyn. 31 (7), 869–893.

Barrett, T.J., Anderson, G.M., Lugowski, J., 1988. The solubility of hydrogen sulphide in 0–5 m NaCl solutions at 25°–95°C and one atmosphere. Geochim.Cosmochim.Acta 52 (4), 807–811. 10.1016/0016-7037(88)90352-3.

Barta, L., Bradley, D.J., 1985. Extension of the specific interaction model to include gas solubilities in high temperature brines. Geochim.Cosmochim.Acta 49 (1), 195–203. 10.1016/0016-7037(85)90204-2.

Ben-Naim, A., 1978. A simple model for demonstrating the relation between solubility, hydrophobic interaction, and structural changes in the solvent. J. Phys. Chem. 82 (8), 874–885. 10.1021/j100497a007.

Berendsen, H.J.C., Grigera, J.R., Straatsma, T.P., 1987. The missing term in effective pair potentials. J. Phys. Chem. 91 (24), 6269–6271. 10.1021/j100308a038.

Beutler, T.C., Mark, A.E., Vanschaik, R.C., Gerber, P.R., Vangunsteren, W.F., 1994. Avoiding Singularities and Numerical Instabilities in Free-Energy Calculations Based on Molecular Simulations. Chemical Physics Letters 222 (6), 529–539.

Burgess, M.P., German, R.P., 1969. Physical Properties of Hydrogen Sulfide - Water Mixtures. AIChE J. 15, 272–275.

Chandrasekhar, J., Spellmeyer, D.C., Jorgensen, W.L., 1984. Energy component analysis for dilute aqueous solutions of lithium(1+), sodium(1+), fluoride(1-), and chloride(1-) ions. J. Am. Chem. Soc. 106 (4), 903–910. 10.1021/ja00316a012.

Chang, J., 2009. The calculation of chemical potential of organic solutes in dense liquid phases by using expanded ensemble Monte Carlo simulations. J.Chem.Phys. 131 (7).

Chapoy, A., Mohammadi, A.H., Tohidi, B., Valtz, A., Richon, D., 2005. Experimental measurement and phase behavior modeling of hydrogen sulfide-water binary system. Ind.Eng.Chem.Res. 44 (19), 7567–7574.

Chen, A.A., Pappu, R.V., 2007. Quantitative Characterization of Ion Pairing and Cluster Formation in Strong 1:1 Electrolytes. J. Phys. Chem. B 111 (23), 6469–6478. 10.1021/jp0708547.

Chialvo, A.A., Simonson, J.M., 2007. Ion pairing and counterion condensation in aqueous electrolyte and polyelectrolyte solutions: Insights from molecular simulation. EMLG/JMLG 2005 Special IssueAnnual Meeting of the EMLG/JMLG 2005 134 (1–3), 15–22. 10.1016/j.molliq.2006.12.017.

Degreve, L.É., Mazzé, F.M., 2003. Molecular simulation of LiCl aqueous solutions. Molecular Physics 101 (10), 1443–1453. 10.1080/0026897031000092256.

Delhommelle, J., Millie, P., 2001. Inadequacy of the Lorentz-Berthelot combining rules for accurate predictions of equilibrium properties by molecular simulation. Mol.Phys. 99, 619–625.

douabul, A.A., Riley, J.P., 1979. The Solubility of Gases in Distilled Water and Seawater - V. Hydrogen Sulfide. Deep-Sea Res. 26, 259–268.

Drummond, D., 1981. Boiling and Mixing of Hydrothermal Fluids: Chemical Effects on Mineral Precipitation. PhD Thesis, Pennsylvania State University, State College, PA.

Duan, Z., Moller, N., Weare, J.H., 1996. Prediction of the solubility of H2S in NaCl aqueous solution: an equation of state approach. Chem.Geol. 130, 15–20.

500 Duan, Z., Sun, R., Liu, R., Zhu, C., 2007. Accurate Thermodynamic Model for the Calculation of H2S
501 Solubility in Pure Water and Brines. Energy Fuels 21 (4), 2056–2065. 10.1021/ef070040p.
502 Dubessy, J., Tarantola, A., Sterpenich, J., 2005. Modelling of Liquid-Vapour Equilibria in the H2O-CO2-
503 NaCl and H2O-H2S-NaCl Systems to 270°C. Oil & Gas Science and Technology - Rev.IFP 60, 339–
504 355.
505 Economou, I.G., Garrido, N.M., Makrodimitri, Z.A., 2010. Prediction of microscopic structure and
506 physical properties of complex fluid mixtures based on molecular simulation. Fluid Phase Equilib.
507 296, 125–132. 10.1016/j.fluid.2010.09.040.
508 Frenkel, D., Smit, B., 1996. Understanding Molecular Simulation: From Algorithms to Applications.
509 Academic Press, San Diego.
510 Garrido, N.M., Queimada, A.J., Jorge, M., Economou, I.G., Macedo, E.A., 2010. Molecular simulation
511 of absolute hydration Gibbs energies of polar compounds. Fluid Phase Equilib. 296 (2), 110–115.
512 Garrido, N.M., Queimada, A.J., Jorge, M., Macedo, E.A., Economou, I.G., 2009. 1-Octanol/Water
513 Partition Coefficients of n-Alkanes from Molecular Simulations of Absolute Solvation Free
514 Energies. Journal of Chemical Theory and Computation 5 (9), 2436–2446.
515 Gerrard, W., 1972. Solubility of Hydrogen Sulfide, Dimethyl Ether, Methyl Chloride, and Sulfur
516 Dioxide in Liquids. The Prediction of Solubility of All Gases. J. Appl. Chem. Biotechnol. 22, 623–
517 650.
518 Harvey, A.H., 1996. Semiempirical correlation for Henry's constants over large temperature ranges.
519 AIChE J. 42, 1491–1494.
520 Impey, R.W., Madden, P.A., McDonald, I.R., 1983. Hydration and mobility of ions in solution: The
521 Journal of Physical Chemistry. The Journal of Physical Chemistry 87 (25), 5071–5083.
522 10.1021/j150643a008.
523 Ji, Q., Pellenq, R., van Vliet, K., 2012. Comparison of computational water models for simulation of
524 calcium–silicate–hydrate. Computational Materials Science 53 (1), 234–240.
525 10.1016/j.commatsci.2011.08.024.
526 Jiang, H., Mester, Z., Moultos, O.A., Economou, I.G., Panagiotopoulos, A.Z., 2015. Thermodynamic
527 and Transport Properties of H2O + NaCl from Polarizable Force Fields. J. Chem. Theory Comput.
528 11 (8), 3802–3810. 10.1021/acs.jctc.5b00421.
529 Jiang, H., Moultos, O.A., Economou, I.G., Panagiotopoulos, A.Z., 2016. Hydrogen-Bonding Polarizable
530 Intermolecular Potential Model for Water. J. Phys. Chem. B 120 (48), 12358–12370.
531 10.1021/acs.jpcb.6b08205.
532 Kiss, P.T., Baranyai, A., 2014. A new polarizable force field for alkali and halide ions. J.Chem .Phys.
533 141, 114501.
534 Kiss, P.T., Bertsyk, P., Baranyai, A., 2012a. Testing recent charge-on-spring type polarizable water
535 models. I. Melting temperature and ice properties. J.Chem .Phys. 137, 194102.
536 Kiss, P.T., Darvas, M., Baranyai, A., Jedlovszky, P., 2012b. Surface properties of the polarizable
537 Baranyai-Kiss water model. J.Chem .Phys. 136, 114706.
538 Kong, C.L., 1973. Combining rules for intermolecular potential parameters. II. Rules for the Lennard-
539 Jones (12-6) potential and the Morse potential. J.Chem.Phys. 59, 2464.
540 Koschel, D., Coxam, J.Y., Majer, V., 2013. Enthalpy and Solubility Data of H2S in Aqueous Salt
541 Solutions at Conditions of Interest for Geological Sequestration. Ind. Eng. Chem. Res. 52, 14483–
542 14491.

543 Koschel, D., Coxam, J.-Y., Majer, V., 2007. Enthalpy and Solubility Data of H2S in Water at Conditions
544 of Interest for Geological Sequestration. Ind. Eng. Chem. Res. 46 (4), 1421–1430.
545 10.1021/ie061180.
546 Kozintseva, T.N., 1963. Solubility of Hydrogen Sulfide in Water and on Salt Solutions at Elevated
547 Temperatures. In: Geokhimischskie issledovaniya v oblasti povyshennykh davlenii i temperatur.
548 Khitarova, N. I., Ed; Akademiia Nauk, Moscow.
549 Kristof, T., Liszi, J., 1997. Effective intermolecular potential for fluid hydrogen sulfide. J.Phys.Chem.B
550 101 (28), 5480–5483.
551 Kuranov, G., Rumpf, B., Smirnova, N.A., Maurer, G., 1996. Solubility of single gases carbon dioxide
552 and hydrogen sulfide in aqueous solutions of N-methyldiethanolamine in the temperature range
553 313-413 K at pressures up to 5 MPa. Ind.Eng.Chem.Res. 35 (6), 1959–1966.
554 Lamoureux, G., Roux, B., 2006. Absolute Hydration Free Energy Scale for Alkali and Halide Ions
555 Established from Simulations with a Polarizable Force Field. J. Phys. Chem. B 110 (7), 3308–3322.
556 10.1021/jp056043p.
557 Lee, J.I., Mather, A.E., 1977. Solubility of Hydrogen Sulfide in water. Berichte der Bunsen-Gesellschaft
558 f_r Physikalische Chemie 81 (10), 1021–1023.
559 Lee, S.H., Rasaiah, J.C., 1996. Molecular Dynamics Simulation of Ion Mobility. 2. Alkali Metal and
560 Halide Ions Using the SPC/E Model for Water at 25 -¦CÔÇá: The Journal of Physical Chemistry.
561 The Journal of Physical Chemistry 100 (4), 1420–1425. 10.1021/jp953050c.
562 Li, J., Wei, L., Li, X., 2014. Modeling of CO2-CH4-H2S-brine based on cubic EOS and fugacity-activity
563 approach and their comparisons. 12th International Conference on Greenhouse Gas Control
564 Technologies, GHGT-12 63, 3598–3607. 10.1016/j.egypro.2014.11.390.
565 Li, J., Wei, L., Li, X., 2015. An improved cubic model for the mutual solubilities of CO2–CH4–H2S–brine
566 systems to high temperature, pressure and salinity. Applied Geochemistry 54, 1–12.
567 10.1016/j.apgeochem.2014.12.015.
568 Lísal, M., Smith, W.R., Kolafa, J., 2005. Molecular Simulations of Aqueous Electrolyte Solubility: 1.
569 The Expanded-Ensemble Osmotic Molecular Dynamics Method for the Solution Phase. J. Phys.
570 Chem. B 109 (26), 12956–12965. 10.1021/jp0507492.
571 Liu, Y., Lafitte, T., Panagiotopoulos, A.Z., Debenedetti, P.G., 2013. Simulations of vapor–liquid phase
572 equilibrium and interfacial tension in the CO2–H2O–NaCl system. AIChE J. 59 (9), 3514–3522.
573 10.1002/aic.14042.
574 Lyubartsev, A.P., Laaksonen, A., 1996. Concentration Effects in Aqueous NaCl Solutions. A Molecular
575 Dynamics Simulation. J. Phys. Chem. 100 (40), 16410–16418. 10.1021/jp961317h.
576 MAchel, H.G., 2001. Bacterial and thermochemical sulfate reduction in diagenetic settings -old and
577 new insights. Sedimentary Geology 140, 143–175.
578 Mackie, A.D., Tavitian, B., Boutin, A., Fuchs, A.H., 1997. Vapour-liquid phase equilibria predictions of
579 methane-alkane mixtures by Monte Carlo simulation. Mol.Sim. 19 (1), 1–15.
580 Marcus, Y., 1988. Ionic radii in aqueous NaCl solutions. Chem.Rev. 88 (1475-1498).
581 Megyes, T., Bakó, I., Bálint, S., Grósz, T., Radnai, T., 2006. Ion pairing in aqueous calcium chloride
582 solution: Molecular dynamics simulation and diffraction studies. New Highlights of Solution
583 Chemistry: Diffraction, Simulation and Theoretical StudiesInvited Contributions Dedicated to
584 Professor Gabor Palinkas on Occasion on his 65th Birthday 129 (1–2), 63–74.
585 10.1016/j.molliq.2006.08.013.
586 Mester, Z., Panagiotopoulos, A.Z., 2015. Mean ionic activity coefficients in aqueous NaCl solutions
587 from molecular dynamics simulations. J.Chem .Phys. 142, 44507.

588 Misztal, R., Sangwal, K., 1999. Analysis of the Concentration and Temperature Dependence of
589 Densities of Aqueous Alkali Halide Solutions: a New Power-Law Approach. Crystal Research and
590 Technology 34, 769–775.
591 Moucka, F., Nezbeda, I., Smith, W.R., 2013. Molecular force fields for aqueous electrolytes: SPC/E-
592 compatible charged LJ sphere models and their limitations. J.Phys.Chem 138, 154102.
593 Moučka, F., Nezbeda, I., Smith, W.R., 2013. Computationally efficient Monte Carlo simulations for
594 polarisable models: multi-particle move method for water and aqueous electrolytes. Molecular
595 Simulation 39 (14-15), 1125–1134. 10.1080/08927022.2013.804183.
596 Moučka, F., Nezbeda, I., Smith, W.R., 2015. Chemical Potentials, Activity Coefficients, and Solubility in
597 Aqueous NaCl Solutions: Prediction by Polarizable Force Fields. J. Chem. Theory Comput. 11 (4),
598 1756–1764. 10.1021/acs.jctc.5b00018.
599 Neyt, J.-C., Wender, A., Lachet, V., Ghoufi, A., Malfreyt, P., 2013. Prediction of the concentration
600 dependence of the surface tension and density of salt solutions: atomistic simulations using
601 Drude oscillator polarizable and nonpolarizable models. Phys. Chem. Chem. Phys. 15 (28), 11679–
602 11690. 10.1039/C3CP50904D.
603 Orozco, G.A., Moultos, O.A., Jiang, H., Economou, I.G., Panagiotopoulos, A.Z., 2014. Molecular
604 simulation of thermodynamic and transport properties for H2O+NaCl system. J.Chem .Phys. 141,
605 234507.
606 Partay, L., Jedlovszky, P., Jancso, G., 2005. Calculation of the hydration free energy difference
607 between pyridine and its methyl-substituted derivatives by computer simulation methods. The
608 Journal of Physical Chemistry B 109 (16), 8097–8102.
609 Pohl, H. A., 1961. Thermodynamics of the Hydrogen Sulfide-Water-System Relevant to the Dual
610 Temperature Process for the Production of Heavy Water. J. Chem. Eng. Data 6 (4), 515–521.
611 10.1021/je60011a010.
612 Rick, S.W., Stuart, S.J., Berne, B.J., 1994. Dynamic fluctuating charge force fields: application to liquid
613 water. J.Chem .Phys. 101, 6141.
614 Rinker, E.B., Sandall, O.C., 2000. Physical solubility of hydrogen sulfide in several aqueous solvents.
615 Can.J.Chem.Eng. 78 (1), 232–236.
616 Romankiw, L.A., Chou, I.M., 1983. Densities of Aqueous Sodium Chloride, Potassium Chloride,
617 Magnesium Chloride, and Calcium Chloride Binary Solutions in the Concentration Range 0.5-6.1
618 M at 25, 30, 35, 40, and 45 C. J.Chem.Eng.Data 28 (3), 300–305.
619 Savary, V., Berger, G., Dubois, M., Lacharpagne, J.-C., Pages, A., Thibeau, S., Lescanne, M., 2012. The
620 solubility of CO2 + H2S mixtures in water and 2 M NaCl at 120 °C and pressures up to 35 MPa.
621 International Journal of Greenhouse Gas Control 10, 123–133. 10.1016/j.ijggc.2012.05.021.
622 Selleck, F.T., Carmichael, L.T., Sage, B.H., 1952. Phase behavior in the hydrogen sulfide-water system.
623 Ind.Eng.Chem.Res. 44 (9), 2219–2226.
624 Setschenow, J.Z., 1889. Uber die konstitution der saltzosungenauf grund ihres verhaltens zu
625 kohlensaure. Z.Physik.Chemie 4, 117–125.
626 Shirts, M.R., Pitera, J.W., Swope, W.C., Pande, V.S., 2003. Extremely precise free energy calculations
627 of amino acid side chain analogs: Comparison of common molecular mechanics force fields for
628 proteins. J.Chem.Phys. 119 (11), 5740–5761.
629 Soave, G., 1972. Equilibrium Constants for a Modified Redlich-Kwong Equation of State. Chemical
630 Engineering Science 27, 1197–1203.
631 Soreide, I., Whitson, C., 1992. Peng-Robinson predictions for hydrocarbons, CO_2, N_2, and H_2S with
632 pure water and NaCl brine. Fluid Phase Equilib. 77, 217–240.

633 Suleimenov, O.M., Krupp, R.E., 1994. Solubility of hydrogen sulfide in pure water and in NaCl
634 solutions, from 20 to 320°C and at saturation pressures. Geochim.Cosmochim.Acta 58 (11),
635 2433–2444. 10.1016/0016-7037(94)90022-1.
636 Sun, W., Nešić, S., Young, D., Woollam, R.C., 2008. Equilibrium Expressions Related to the Solubility of
637 the Sour Corrosion Product Mackinawite. Ind. Eng. Chem. Res. 47 (5), 1738–1742.
638 10.1021/ie070750i.
639 Theodorou, D.N., 2010. Progress and Outlook in Monte Carlo Simulations. Ind.Eng.Chem.Res. 49,
640 3047–3058.
641 Trinh, T.-K.-H., Hemptinne, J.-C. de, Lugo, R., Ferrando, N., Passarello, J.-P., 2016. Hydrogen Solubility
642 in Hydrocarbon and Oxygenated Organic Compounds. J. Chem. Eng. Data 61 (1), 19–34.
643 10.1021/acs.jced.5b00119.
644 Tsai, E.S., Jiang, H., Panagiotopoulos, A.Z., 2016. Monte Carlo simulations of H2O-CaCl2 and H2O-
645 CaCl2-CO2 mixtures. Fluid Phase Equilib. 407, 262–268.
646 Ungerer, P., Tavitian, B., Boutin, A., 2005. Applications of Molecular Simulation in the Oil and Gas
647 Industry. Editions Technip.
648 Ungerer, P., Wender, A., Demoulin, G., Bourasseau, E., Mougin, P., 2004. Application of Gibbs
649 Ensemble and NPT Monte Carlo Simulation to the Development of Improved Processes for H2S-
650 rich Gases. Mol.Sim. 30 (10), 631–648.
651 Vorholz, J., Harismiadis, V.I., Panagiotopoulos, A.Z., Rumpf, B., Maurer, G., 2004. Molecular
652 Simulation of the Solubility of Carbon Dioxide in Aqueous Solutions of Sodium Chloride. Fluid
653 Phase Equilib. 226, 237–250.
654 Waldmann, M., Hagler, A.T., 1993. New combining rules for rare gas van der waals parameters.
655 J.Comput.Chem. 14, 1077–1084.
656 Wang, P., Anderko, A., 2001. Computation of dielectric constants of solvent mixtures and electrolyte
657 solutions. Fluid Phase Equilib. 186, 103–122.
658 Widom, B., 1963. Some topics in the theory of fluids. J.Chem.Phys. 39, 2808–2812.
659 Xia, J., Pérez-Salado Kamps, Á., Rumpf, B., Maurer, G., 2000. Solubility of Hydrogen Sulfide in
660 Aqueous Solutions of the Single Salts Sodium Sulfate, Ammonium Sulfate, Sodium Chloride, and
661 Ammonium Chloride at Temperatures from 313 to 393 K and Total Pressures up to 10 MPa. Ind.
662 Eng. Chem. Res. 39 (4), 1064–1073. 10.1021/ie990416p.
663 Yu, H., Whitfield, T.W., Harder, E., Lamoureux, G., Vorobyov, I., Anisimov, V.M., MacKerell, A.D.,
664 Roux, B., 2010. Simulating Monovalent and Divalent Ions in Aqueous Solution Using a Drude
665 Polarizable Force Field. J. Chem. Theory Comput. 6 (3), 774–786. 10.1021/ct900576a.
666 Yu, Q., Liu, D., Liu, R., Zhou, H., Chen, M., Chen, G., Chen, Y., Hu, Y., Xu, X., Shen, L., Han, S.J., 1980.
667 VLE of H2S-H2O System. Huagong Xuebao 4, 1–7.
668 Zhang, Han, 1996. Viscosity and Density of Water + Sodium Chloride + Potassium Chloride Solutions
669 at 298.15 K. J. Chem. Eng. Data 41 (3), 516–520. 10.1021/je9501402.
670 Ziabakhsh-Ganji, Z., Kooi, H., 2012. An Equation of State for thermodynamic equilibrium of gas
671 mixtures and brines to allow simulation of the effects of impurities in subsurface CO2 storage.
672 CATO: CCS Research in the Netherlands 11, Supplement, S21-S34. 10.1016/j.ijggc.2012.07.025.
673 Zirrahi, M., Azin, R., Hassanzadeh, H., Moshfeghian, M., 2012. Mutual solubility of CH4, CO2, H2S,
674 and their mixtures in brine under subsurface disposal conditions. Fluid Phase Equilibria 324, 80–
675 93. 10.1016/j.fluid.2012.03.017.

Table 1. Parameters of correlation **Error! Reference source not found.** for the Henry constant of H_2S in pure water.

a_i	b_i	c_i
-1.67464	8.53988	-1.18646

Table 2. Details of molecular models used

Molecule	Force center or charge	Position (Å)			Lennard-Jones parameters		Charge
		X	*Y*	*Z*	σ (Å)	ε/k (K)	*q* (e)
H_2O	O	0	0	0	3.1655	78.2	-0.8476
	H1	0.8165	0.5774	0	0	0	0.4238
	H2	-0.8165	0.5774	0	0	0	0.4238
H_2S	S	0	0	0	3.7300	250.0	-0.4
	H1	0.9639	0.9308	0	0	0	0.25
	H2	-0.9639	0.9308	0	0	0	0.25
	M	0	0.1862	0	0	0	-0.9
Na^+	Na	0	0	0	1.8974	808.7	1
Cl^-	Cl	0	0	0	4.4172	59.3	-1

Table 3. Evaluated combining rules for the binary system $H_2S + H_2O$

Lorentz-Berthelot	Kong	Waldmann-Hagler
$\varepsilon_{ij} = \sqrt{\varepsilon_i \varepsilon_j}$ $\sigma_{ij} = \frac{\sigma_i + \sigma_j}{2}$	$\varepsilon_{ij}\sigma_{ij}^6 = \sqrt{\varepsilon_i \sigma_i^6 \varepsilon_j \sigma_j^6}$ $\varepsilon_{ij}\sigma_{ij}^{12} = \frac{\varepsilon_i \sigma_i^{12}}{2^{13}}\left[1+\left(\frac{\varepsilon_j \sigma_j^{12}}{\varepsilon_i \sigma_i^{12}}\right)^{\frac{1}{13}}\right]^{13}$	$\varepsilon_{ij}\sigma_{ij}^6 = \sqrt{\varepsilon_i \sigma_i^6 \varepsilon_j \sigma_j^6}$ $\sigma_{ij} = \left(\frac{\sigma_i^6 + \sigma_j^6}{2}\right)^{\frac{1}{6}}$

Table 4. Average deviations (%) between experimental (Koschel et al., 2013; Xia et al., 2000) and calculated H_2S Henry constants in NaCl aqueous solutions from 0 to 6 mol/kg.

T (K)	without k_{ij}	with $k_{ij}(H_2S\text{-}H_2O)$ = -0.16
323.15	72.8	39.4
353.15	171.0	34.5
393.16	183.2	38.5

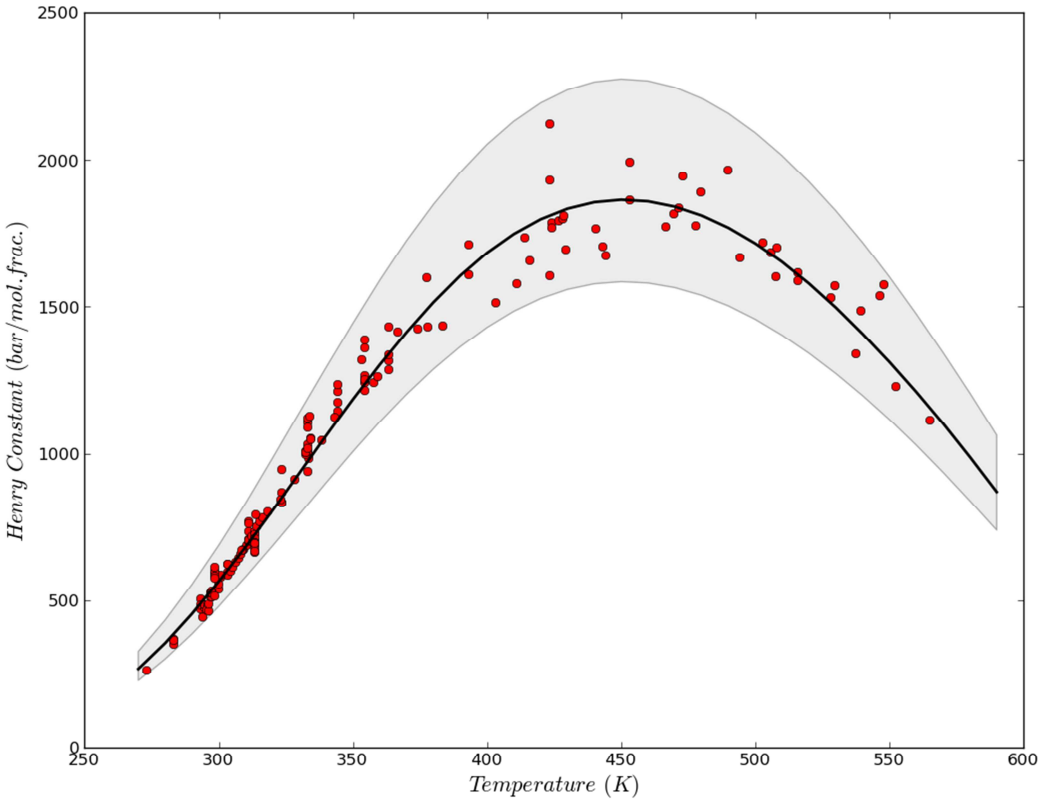

Figure 1. Experimental (symbols) and correlated (bold line) Henry constants of H_2S in pure water; the shaded grey area highlights the experimental uncertainties.

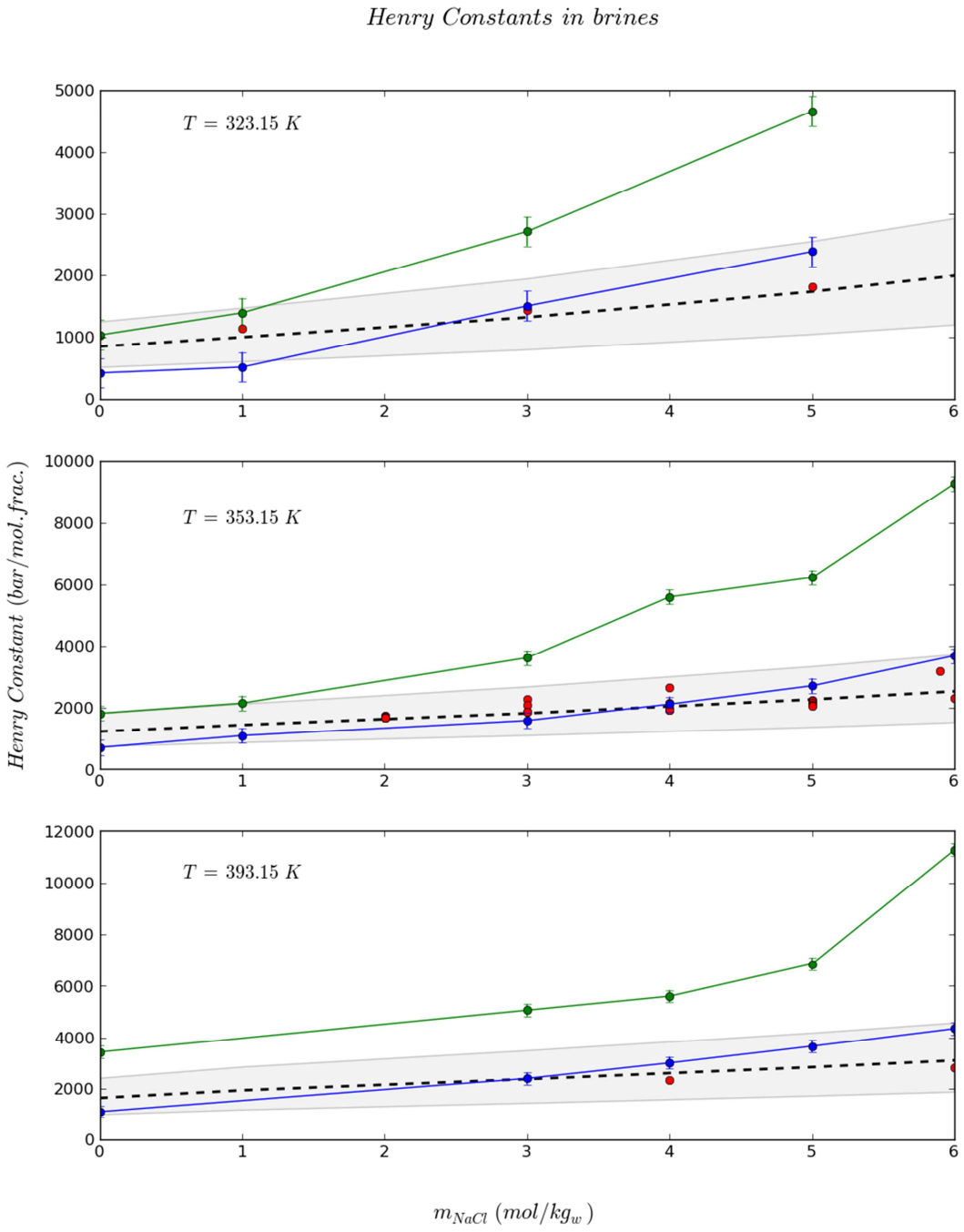

Figure 10. Henry constant of H_2S in NaCl aqueous solutions at 323.15 K (a), 353.15 K (b) and 393.15 K (c). The Monte Carlo simulation results obtained with the predicted approach without k_{ij} are in green, while the ones obtained with the approach using the optimized H_2S-H_2O k_{ij} are in blue. For each molality, the available experimental data are plotted (red dots). The dashed line is the correlated Henry constant of H_2S in aqueous solutions calculated according the approach described in section 2.2. The shaded grey area shows the minimal uncertainty associated to the experimental measurements.

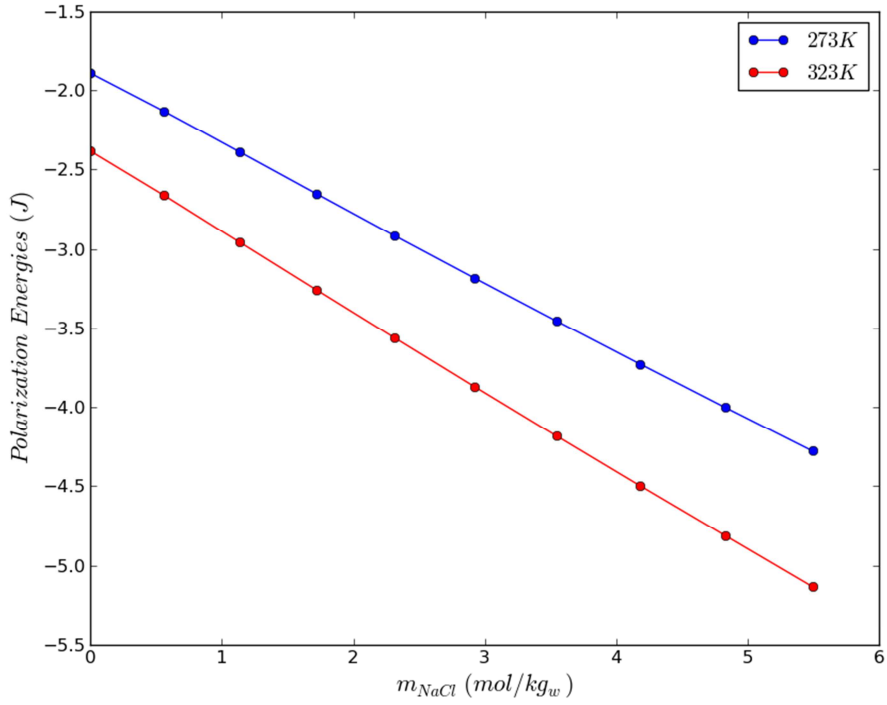

Figure 11. Assessment of the polarization energy due to cations and anions in a NaCl aqueous solution as a function of the ionic concentration at 273 K and 323 K

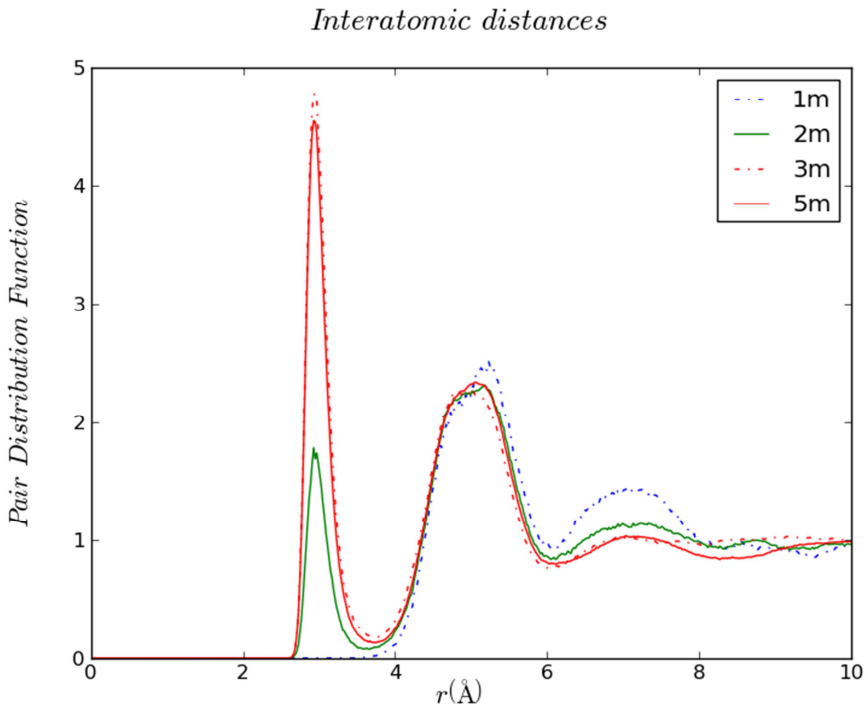

Figure 12. Radial distribution functions for Na^+-Cl^- ionic pairs in a NaCl aqueous solution for molality ranging from 1 to 5 mol/kg.

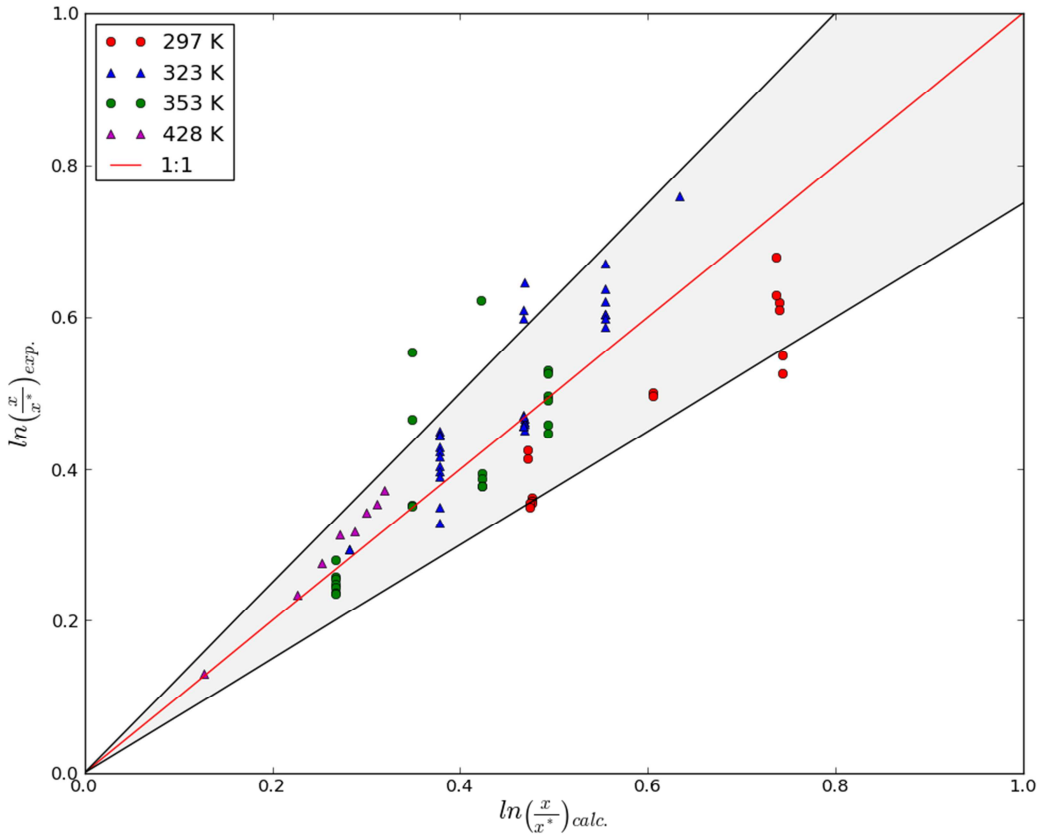

Figure 2. Ratio of H_2S solubility in pure water *x* and in aqueous NaCl solution *x* as a function of NaCl concentration at 298.15 K (red circles)(Barrett et al., 1988), 333.15 K (blue triangles) (Barrett et al., 1988; Xia et al., 2000), 353.15 K (green circles)(Barrett et al., 1988) and 428.15 K (pink triangles)(Suleimenov and Krupp, 1994).* The shaded grey area corresponds to a relative uncertainty of ±25 %.

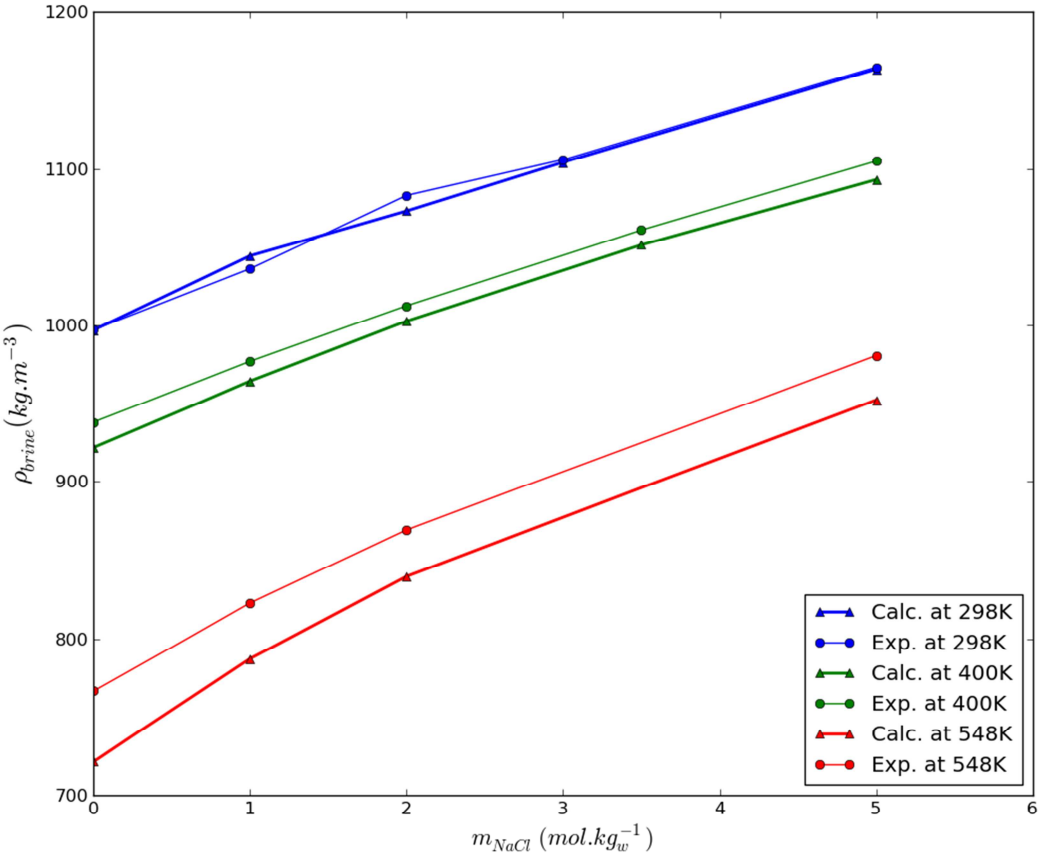

Figure 3. Experimental (circles) (Apelblat and Manzurola, 1999; Zhang and Han, 1996) and calculated (triangles) liquid density of NaCl aqueous solution at 298 K, 400 K and 548 K.

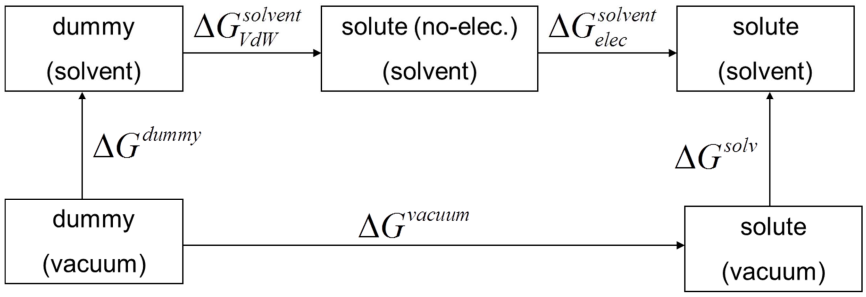

Figure 4. Thermodynamic cycle used to calculate Gibbs energy of solvation.

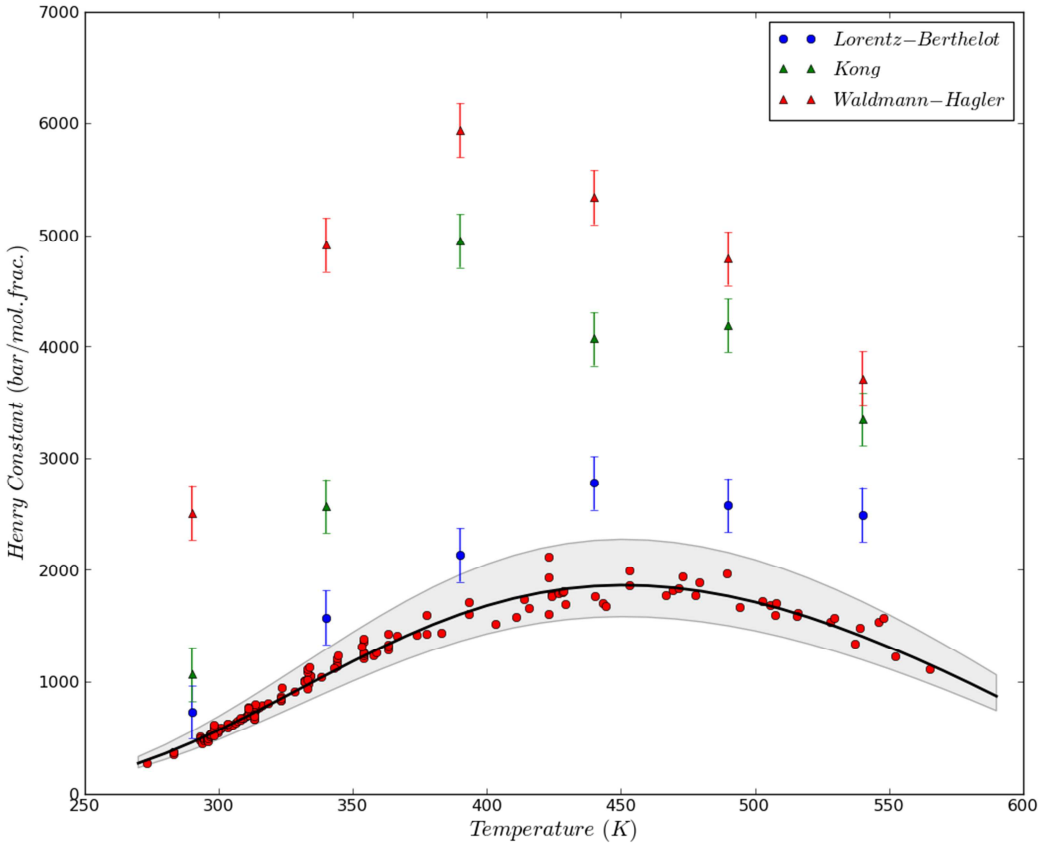

Figure 5. Henry constant of H_2S in pure water: experimental data (red symbols) and correlated (bold line) Henry constants of H_2S in pure water; the shaded grey area highlights the experimental uncertainties; Monte-Carlo simulation results with the combining rule of Lorentz-Berthelot, Kong and Waldmann-Hagler.

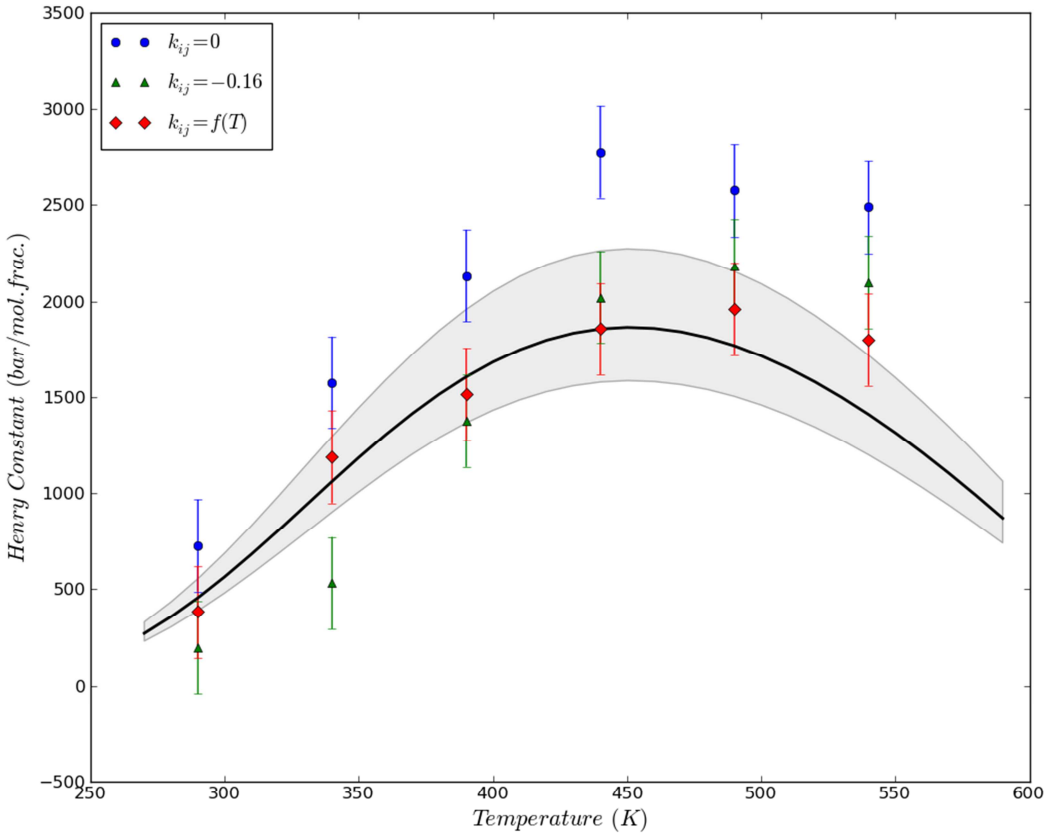

Figure 6. Henry constant of H_2S in pure water with the predictive approach (k_{ij}=0, circles), with the temperature-independent k_{ij} (k_{ij} =-0.16, green triangles), and with the temperature-dependent k_{ij} (equation Error! Reference source not found.**, red triangles). The line represents the correlated experimental data, the shaded grey area highlights the experimental uncertainties.**

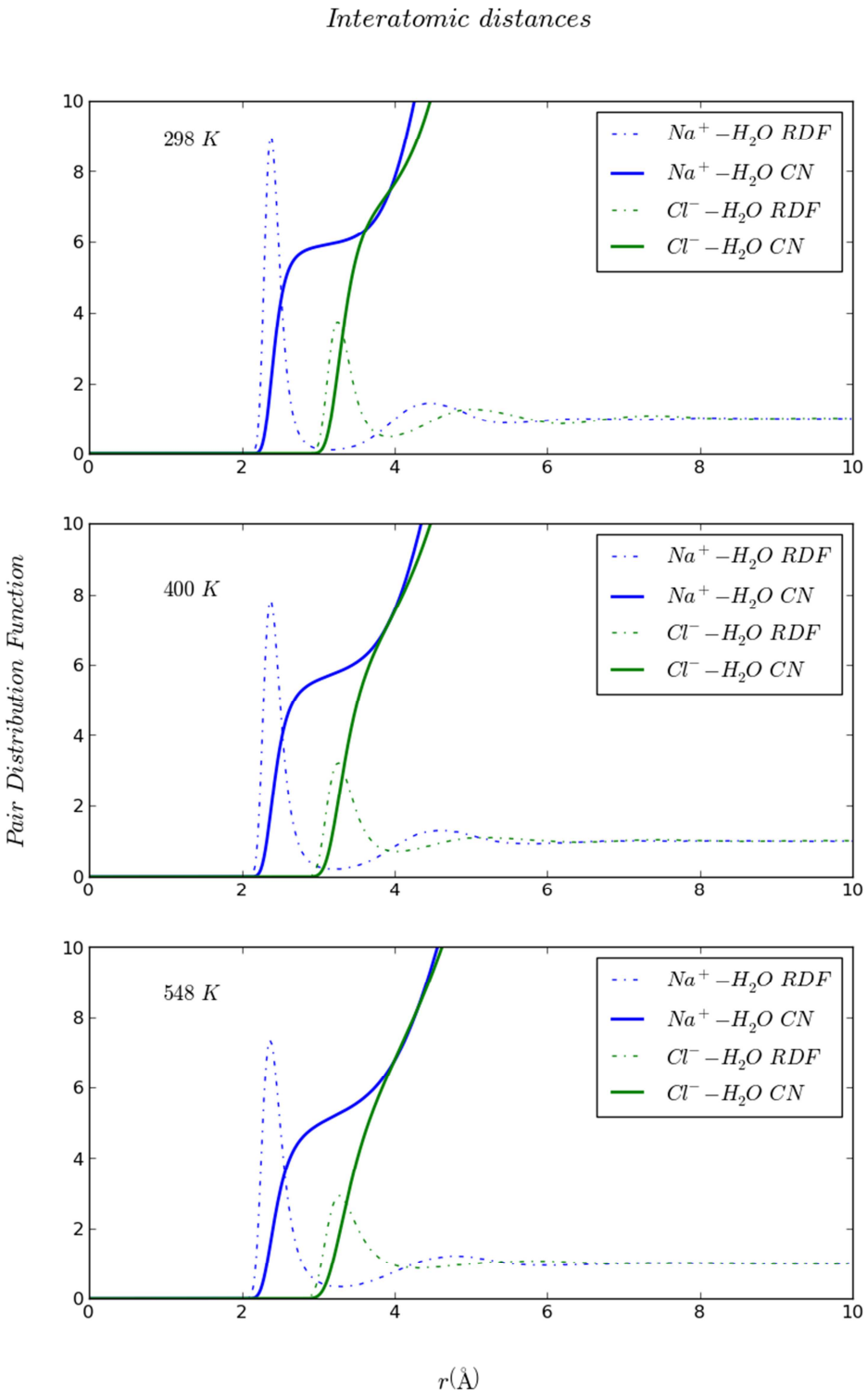

Figure 7. Radial distribution functions (RDF, dotted lines) and coordination numbers (CN, solid lines) for H_2O-Na^+ pairs (in blue) and H_2O-Cl^- pairs (in green) in a NaCl aqueous solution at 1 mol/kg for three temperatures.

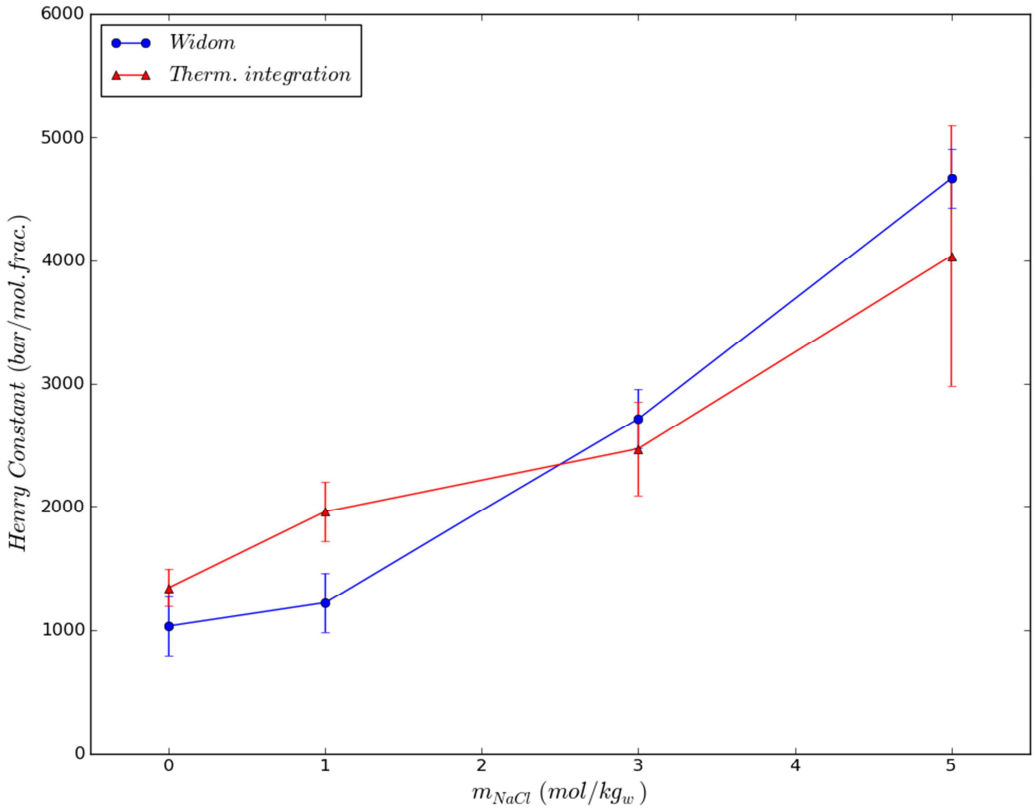

Figure 8. Henry constant of H_2S in aqueous NaCl solutions calculated at 323.15 K either with the Widom particle insertion method or with the thermodynamic integration method.

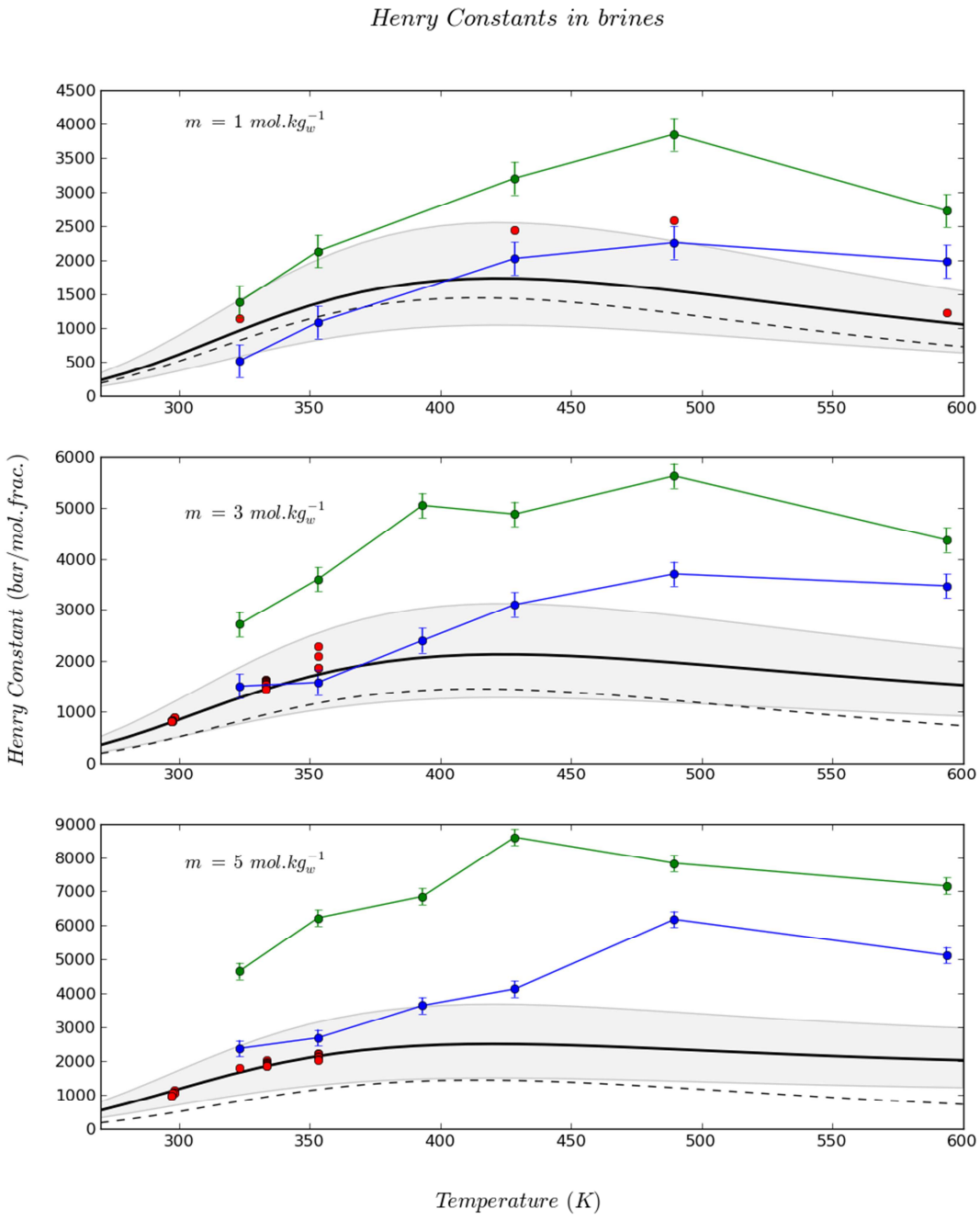

Figure 9. Henry constant of H_2S in NaCl aqueous solutions (1, 3, 5 mol/kg) as a function of the temperature. The Monte Carlo simulation results obtained with the predicted approach without k_{ij} are in green, while the ones obtained with the approach using the optimized H_2S-H_2O k_{ij} are in blue. For each molality, the available experimental data are plotted (red dots). The dash line is the correlated Henry constant of H_2S in pure water (eq. 2). The bold line is the correlated Henry constant of H_2S in aqueous solutions calculated according to the approach described in section 2.2. The shaded grey area shows the minimal uncertainty associated to the experimental measurements.

- Experimental Henry constants data of H_2S in NaCl aqueous solution are compiled from literature and smoothed with a simple correlation.
- A non-polarizable force field is evaluated to predict Henry constant of H_2S in NaCl aqueous solution through Monte Carlo simulations using Widom test insertion and thermodynamic integration methods.
- A temperature-independent interaction binary parameter is adjusted on experimental data and introduced in the force field.
- A good agreement between experimental and calculated Henry constant of H_2S in NaCl aqueous solution is obtained on a large temperature range (290 to 590 K) and salinity range (up to 6 mol/kg).